The dynamics of the $O(^1D)+HD$ reaction: A quasiclassical trajectory multisurface study

Cite as: J. Chem. Phys. **113**, 5339 (2000); https://doi.org/10.1063/1.1290127
Submitted: 17 May 2000 . Accepted: 10 July 2000 . Published Online: 18 September 2000

F. J. Aoiz, L. Bañares, M. Brouard, J. F. Castillo, and V. J. Herrero

The dynamics of the O(^1D)+HD reaction: A quasiclassical trajectory multisurface study

F. J. Aoiz[a] and L. Bañares
Departamento de Química Física, Facultad de Química, Universidad Complutense, 28040 Madrid, Spain

M. Brouard
Physical and Theoretical Chemistry Laboratory, South Parks Road, Oxford OX1 3QZ, United Kingdom

J. F. Castillo
Departamento de Química Física, Facultad de Química, Universidad Complutense, 28040 Madrid, Spain

V. J. Herrero
Instituto de Estructura de la Materia (CSIC), Serrano 123, 28006 Madrid, Spain

(Received 17 May 2000; accepted 10 July 2000)

Integral and differential cross sections for the O(^1D)+HD reaction have been obtained from adiabatic and nonadiabatic quasiclassical trajectory calculations performed on new *ab initio* versions of the $1A'$, $1A''$ and $2A'$ potential energy surfaces at the collision energies of 0.089 and 0.196 eV (2.05 and 4.53 kcal/mol, respectively). Results are reported for both the OH+D and OD+H exit channels of reaction. The new data are compared with those from previous theoretical studies employing other potential energy surfaces, and are also used to simulate experimental differential cross sections obtained from recent molecular beam measurements, which are partially resolved in the internal states of the products. The comparison provides evidence that excited electronic states do participate in the title reaction at 0.196 eV, but that their contribution, particularly that of the A'' state, is overestimated by the quasiclassical trajectory (QCT) calculations employing the latest, and most accurate, potential energy surfaces. © *2000 American Institute of Physics.* [S0021-9606(00)01637-8]

I. INTRODUCTION

The O(^1D)+H_2 reactive system and its deuterated isotopic variants have long been considered as prototypes for barrierless chemical reactions proceeding through an insertion mechanism.[1–34] At the collision energies employed in the majority of experiments (up to ≈0.25 eV), the reactivity is largely governed by the lowest adiabatic potential energy surface (PES), termed $1A'$, which has no barrier for most nuclear geometries. The reaction, however, can (in principle) take place *via* electronically excited potential surfaces, and more recently, much experimental and theoretical effort has been devoted to characterizing the precise details of any excited state participation.[5,7,8,11,13,26,29–34]

The $1A'$ PES of O(^1D)+H_2, which correlates with the ground electronic state of water, is largely attractive, with a deep well at perpendicular geometries. The anisotropy of this potential well favors an insertion of the attacking atom into the H_2 bond, rather than direct collisions of the O(^1D) with either end of the molecule. Numerous theoretical studies of the dynamics, using both quasiclassical trajectory (QCT) and approximate quantum mechanical (QM) methods, have been performed on different versions of the ground adiabatic PES (see for instance Refs. 7, 9, 10, 12, 13, 16–19, 27–29, 31 and the references therein).

The reactivity on the excited surfaces has not been studied so thoroughly. The lowest excited $1A''$ PES, which also correlates adiabatically with ground state reagents and products, has a relatively low collinear barrier (≈0.10 eV) which lies in the entrance channel.[7,11,13,26] Therefore, the dynamics on this PES, which can be accessed at the energies of some of the available experiments, should be very different from that taking place on the ground $1A'$ PES. The next excited adiabatic PES, the $2A'$, which is electronically coupled to the $1A'$, has a barrier of similar height to that on the $1A''$ surface.[26] This PES correlates with ground state reagents, but does not correlate with ground state products, and thus its contribution to reaction can only be *via* nonadiabatic transitions.[29,30] Upper PESs, corresponding to the degenerate Δ state in the collinear configuration, correlate with even more highly electronically excited products, and the only interaction with the lower PESs is *via* Coriolis coupling.

The essential properties of the ground and excited electronic states of the HOH system can be found in the article of Durand and Chapuisat,[3] where the literature up to 1985 is reviewed. An analytical representation of the five reactive PESs correlating with the ^1D state of the oxygen atom obtained using the diatomics-in-molecules (DIM) methodology was reported by Kuntz *et al.*[7] More accurate *ab initio* versions of the two lowest adiabatic PESs $1A'$ and $1A''$ have been published by Ho *et al.*[10] and by Schatz *et al.*,[11] respectively. They are usually referred to as the $1A'$ and $1A''$ K PESs. At the time of its publication, the $1A'$ K PES superseded previous versions of the ground state surface for the O(^1D)+H_2 reaction. Until now, the most ''in depth'' dis-

[a]Electronic mail: aoiz@legendre.quim.ucm.es

cussions about the contribution of the excited state pathway to the reactivity have been based on calculations performed on the K PESs. Recent high level *ab initio* calculations by Dobbyn and Knowles[26] have led to the construction of new surfaces (hereafter DK PESs) for the $1A'$, $1A''$ and $2A'$ electronic states and the electronic coupling between the $1A'$ and $2A'$, which are expected to be the most precise ones to date. The PESs are being used currently in dynamical calculations by various groups,[28–30] but, to our knowledge, no thorough comparisons with experiment have been reported thus far.

The excited electronic states are not expected to play a significant role for collision energies below 0.10 eV, approximately the barrier height on both the $1A''$ and $2A'$ PESs. Accordingly, the thermal rate constants for $O(^1D)+H_2/D_2$ recently measured by Talukdar and Ravishankara[35] at 300 K (which corresponds to an average collision energy of 0.04 eV) could be accounted for well by dynamical calculations performed on the $1A'$ ground state surface alone.[18] However, the dependence of the $O(^1D)+H_2/D_2/HD$ reaction cross sections on collision energy, i.e., the excitation functions, measured by Hsu *et al.*,[23] show a rise at collision energies above $E_{col}=0.10$ eV, which were taken as an indication of the participation of electronically excited PESs. These experimental results were in qualitative agreement with theory, although above $E_{col}>0.10$ eV the rise in the excitation functions for the $O(^1D)+H_2$ and $O(^1D)+HD\rightarrow OD+H$ reactions was more pronounced than that obtained from QCT calculations which included contributions from both the $1A'$ and $1A''$ K PESs.[11,36]

Lee and Liu[34] have recently investigated the effect of reagent rotation on the $O(^1D)+H_2(v=0,j)$ reaction by measuring the excitation functions for the reactions of $O(^1D)+p-H_2$ ($\approx$86% of the molecules in $j=0$) and $O(^1D)+n-H_2$ ($\approx$75% of the molecules in $j=1$) over the 0.022–0.14 eV collision energy range. The authors found that for $E_{col}>0.09$ eV, rotational excitation of the hydrogen molecule to $j=1$ enhances the reactivity. This result is at variance with QCT calculations[11,36] on the K PESs, that predict the reaction cross section on the $1A'$ PES to be almost j independent (consistent with reaction on an essentially barrierless surface), and an appreciable decrease in the reactivity on the $1A''$ PES upon excitation of H_2 to the $j=1$ state. Interestingly, QCT calculations[36] on the DK version of the $1A''$ surface give a larger cross section for the reaction of $O(^1D)$ with $H_2(j=1)$ than with $H_2(j=0)$, which is, at least, in qualitative agreement with experiment.

The contribution of the excited $2A'$ PES to the global reactivity (from nonadiabatic transitions) has been studied by Schatz, Pederson and Kuntz[13] using the trajectory surface hopping (TSH) method on DIM $1A'$, $1A''$ and $2A'$ PESs and the couplings between the $1A'$ and $2A'$ surfaces. These authors found that the cross sections obtained from the trajectories started on the $2A'$ were about half those calculated adiabatically on the $1A''$ PES, and that the product state distributions on the $2A'$ surface were intermediate in character between the $1A'$ and $1A''$ PESs. More recently, Drukker and Schatz[29] have performed approximate QM scattering calculations of electronic and rotational Coriolis, and electronic nonadiabatic coupling effects using the DK $1A'$, $1A''$ and $2A'$ surfaces, and the DIM $2A''$ and $3A'$ surfaces for the $O(^1D)+H_2$ reaction. The authors concluded that even though the Coriolis coupling is significant, inducing a redistribution of population between the fine structure levels of the PESs as the reactants approach, the resulting reaction probability and integral cross sections are very similar to those obtained from a Coriolis decoupled calculation. Therefore, as long as the electronic nonadiabatic coupling between the $1A'$ and $2A'$ PESs is considered, Coriolis coupling effects are not important. The nonadiabatic contribution to the cross sections from the $2A'$ surface was found to be about a half of that from the adiabatic calculations on the $1A''$. In addition, Gray *et al.*[30] have performed adiabatic and nonadiabatic wave packet as well as QCT-TSH calculations for the $O(^1D)+H_2(v=0,j=0)$ at total angular momentum $J=0$ as a function of collision energy on DIM PESs and on the DK PESs. They found that there were small differences between the adiabatic and coupled surface results when the initial state was chosen to be the $1A'$ state and that, at energies above the transition state barrier, the $2A'$ reaction probability was similar to that of $1A''$.

Differential cross sections (DCS) have also been determined experimentally for this reaction. These measurements should provide a more sensitive indicator of contributions to the dynamics from excited state PESs to the global reactivity. DCSs without resolution of product internal states have been determined experimentally by different groups[20,21,24,25] in crossed beam experiments. Che and Liu[21] used Doppler shift measurements in a 1+1 resonance enhanced multiphoton ionization (REMPI) scheme for the detection of the H(D) scattered atoms from the $O(^1D)+HD$ reaction at $E_{col}\approx 0.2$ eV. They found significant forward/backward asymmetry in the two isotopic exit channels. Casavecchia and co-workers[24] used mass spectrometric detection of the OH(OD) molecules for the measurement of angular and velocity distributions of the products of the $O(^1D)+H_2$ reaction at $E_{col}=0.08$ and 0.13 eV and of the $O(^1D)+D_2$ reaction at $E_{col}=0.23$ eV. For the lower collision energies, the angular distributions are forward/backward symmetric, but for the higher ones ($E_{col}>0.1$ eV) a slight asymmetry appears, favoring peaking in the backward hemisphere. After a comparison with QCT calculations on DIM PESs, the authors suggested that this slight asymmetry is related to the presence of an abstraction reaction mechanism evolving on one (or both) of the lowest electronically excited surfaces. Ahmed *et al.*[25] have applied the technique of velocity map imaging to obtain the full double (angle and velocity) DCS of the $O(^1D)+D_2$ reaction at $E_{col}=0.1$ eV. The authors found a strong coupling between the translational energy release and the angular distributions of the scattered products, but at the collision energy employed, no effects attributable to reaction *via* an abstraction mechanism on the excited surfaces could be identified.

Angular distributions resolved in OH(v',j') internal state have also been determined. Alexander *et al.*[16,17] obtained OH state-resolved DCSs for the $O(^1D)+H_2$ reaction at a mean collision energy $E_{col}=0.12$ eV using photon initiation coupled with Doppler-resolved laser induced fluorescence (LIF). These experiments, although specific to a single

rovibrational state of the OH products, possess comparatively low energy and angular resolution. In the more recent study, angular distributions were derived for the OH products born specifically in the $v'=4, N'=1$ state,[17] which QCT calculations on the K A' and A'' PESs had predicted to be generated primarily *via* reaction on the A'' excited state. However, comparison of the experimental results with these calculations suggested that the reactivity at the collision energies employed was essentially governed by the reaction on the $1A'$ surface.

More recently, Hsu *et al.*[22,32,33] have used a Doppler-resolved time-of-flight method to obtain DCSs for the $O(^1D)+HD \rightarrow OH(OD)+D(H)$ reaction. These experiments provided data with high resolution in angle and collision energy, and with partial resolution of the internal states of the products. In these studies, the H and D atom time-of-flight (TOF) profiles were used to derive product translational energy distributions for selected center-of-mass (CM) angles, $P(E_t',\theta)$. Structures in some of the $P(E_t',\theta)$ distributions, observed particularly in those corresponding to scattering into the backward hemisphere, were attributed to contributions from the excited $1A''$ PES. However, the comparison between the experimental $P(E_t',\theta)$ distributions for the reaction yielding OH + D[22] and the simulations derived from QCT calculations employing the $1A'$ and $1A''$ K PESs[31] does not provide clear evidence of the participation of the upper PES to this channel of the reaction; on the contrary, the simulations performed with the DCSs calculated using the ground $(1A')$ state PES alone also display the observed structures and, in fact, bear a closer resemblance to experiment than those which included contributions from both the $1A'$ and $1A''$ PESs. In the most recent experiments of Hsu *et al.*,[32,33] the structures observed in some of the $P(E_t',\theta)$ distributions were again attributed to the contribution of the $1A''$ PES, but this assignment is not clearly born out by the QCT calculations on the K PES reported in that work.

In the present article, we report a thorough QCT study of the dynamics of the $O(^1D)+HD \rightarrow OH(OD)+D(H)$ reaction using the $1A'$ DK PESs[26] at two of the collision energies of the experiments of Hsu *et al.*,[32,33] namely $E_{col}=0.089$ and 0.196 eV. At the latter energy, the calculations have also been performed on the $1A''$ and $2A'$ DK PESs. Nonadiabatic contributions from the $2A'$ surface have been taken into account within a trajectory surface hopping (TSH) formalism. The results are compared with the measurements of Hsu *et al.*,[32,33] and with QCT calculations on the K PES, and are discussed in terms of relevant topological features of the PESs involved.

II. METHOD

The quasiclassical trajectory methods employed here are similar to those described in previous publications (see, for instance, Ref. 37 and references therein), and only those details relevant to the present work will be given in this section. The QCT calculations were performed on the DK $1A'$, $1A''$ and $2A'$ surfaces.

A batch of 220 000 trajectories was run on the $1A'$ DK PES at $E_{col}=0.089$ eV (2.05 kcal/mol) and two batches of $\approx$400 000 trajectories each were run on the $1A'$ and $1A''$ DK PESs, respectively, at $E_{col}=0.196$ eV (4.53 kcal/mol). In all batches, the initial rotational quantum number of the HD reactant, j, was randomly sampled according to a Boltzmann distribution at 50 K (81% of $j=0$ and 19% of $j=1$).[22,32,33] Trajectories were started at an $O(^1D)$-HD distance of 8 Å and a time step of 0.02 fs was used. Under these conditions total energy was conserved to better than 1 in 10^5. The maximum impact parameters employed were 2.9 Å ($E_{col}=0.089$ eV) and 2.6 Å ($E_{col}=0.196$ eV), for the $1A'$ and 2.0 Å for the $1A''$ DK PESs, respectively.

As in our previous studies,[37] the rovibrational energies of the HD, OH and OD molecules were calculated by semiclassical quantization of the classical action, using in each case the asymptotic diatomic potential of the PESs. The assignment of final product quantum numbers was carried out by equating the square of the rotational angular momentum of the outgoing diatom to $j'(j'+1)\hbar^2$. With the real values so obtained, the vibrational quantum number v' was found by equating the internal energy of the diatom to the corresponding Dunham expansion. The derived values of v' and j' were then rounded to the nearest integer.

To consider the dynamics on the $1A'$ and $2A'$ DK nonadiabatically coupled potential energy surfaces, we have used a trajectory surface hopping (TSH) method.[38–40] Two batches of 300 000 trajectories were run starting on the $1A'$ or on the $2A'$ DK PESs with the same initial conditions as in the adiabatic calculations on the $1A'$ and $1A''$, respectively. At each time step, every trajectory was checked to see whether a point of intersection between the $1A'$ and $2A'$ surfaces in the diabatic representation had been reached. If so, the Landau-Zener formula was used to compute the probability P_{12} of transition from one adiabatic surface to the other. Following Stine and Muckerman,[38] the Landau-Zener expression employed is

$$P_{12}=\exp(-2\pi\gamma/\hbar), \quad \gamma=\frac{H_{12}^2}{|(dw/dt)_0|}, \tag{1}$$

where H_{12} is the nondiagonal electronic Hamiltonian matrix element between $1A'$ and $2A'$ diabatic DK PESs and $w=H_{22}-H_{11}$, where H_{ii} are the diagonal electronic Hamiltonian matrix elements. As proposed by Miller and George,[41] we have used

$$(dw/dt)_0=A[2-(1\mp 2H_{12}B/A^2)^{1/2}], \tag{2}$$

where

$$A=\sum_{i=1}^{3}\left[\left(\frac{\partial w}{\partial q_i}\right)_0\frac{1}{\mu_{BC}}p_i^{(1)}+\left(\frac{\partial w}{\partial Q_i}\right)_0\frac{1}{\mu_{A,BC}}P_i^{(1)}\right], \tag{3}$$

$$B=\sum_{i=1}^{3}\left[\frac{1}{\mu_{BC}}\left(\frac{\partial w}{\partial q_i}\right)_0^2+\frac{1}{\mu_{A,BC}}\left(\frac{\partial w}{\partial Q_i}\right)_0^2\right], \tag{4}$$

and $\{q_i, Q_i, p_i^{(1)}, P_i^{(1)}, i=1,2,3\}$ are the generalized internal and relative coordinates and momenta before the transition. The subindex 0 refers to the derivatives calculated at the

crossing point. The prescription for changing momenta in order to conserve total energy and angular momentum when a hop occurs at a crossing seam is given by

$$p_i^{(2)} = p_i^{(1)} - \left(\frac{\partial w}{\partial q_i}\right)_0 \frac{A}{B}\left[1 - \left(1 \mp 4H_{12}\frac{B}{A^2}\right)^{1/2}\right], \quad (5)$$

$$P_i^{(2)} = P_i^{(1)} - \left(\frac{\partial w}{\partial Q_i}\right)_0 \frac{A}{B}\left[1 - \left(1 \mp 4H_{12}\frac{B}{A^2}\right)^{1/2}\right]. \quad (6)$$

The following algorithm was applied to take a hopping decision:[38] a random number $\xi \in [0,1]$ was generated, and if $\xi < P_{12}$ the trajectory was made to hop to the other adiabatic surface, and if $\xi \geqslant P_{12}$ the trajectory was allowed to continue on the same adiabatic surface.

As discussed by Schatz *et al.*[13] in a previous TSH study of the $O(^1D) + H_2$ reaction, it is desirable to avoid hops in the asymptotic region where the two surfaces are degenerated. In the case of the $1A'$ and $2A'$ DK PESs, we have found that the diabatic surfaces cross at some points in the asymptotic region. To avoid the asymptotic hopping we have set P_{12} to zero for atom-diatom separations larger than 1.9 Å. In order to gain some insight about the TSH dynamics, an analysis of the hops as a function of the bond angles $\widehat{OHD}$, $\widehat{ODH}$ and $\widehat{HOD}$ has been carried out. Whenever a hop took place, the bond angles were calculated and the trajectory number saved. The hops were then classified according to the value of the bond angles; that is, $90° \leqslant \widehat{OHD} \leqslant 180°$, $90° \leqslant \widehat{ODH} \leqslant 180°$ and $90° \leqslant \widehat{HOD} \leqslant 180°$. This information revealed that surface hopping occurs predominantly around collinear configurations.

DCSs were calculated systematically for every rovibrational state of the OH and OD products by the method of moments expansion in Legendre polynomials. The Smirnov-Kolmogorov test was used to decide when to truncate the series. Significance levels higher than 99% could be achieved using 4–12 moments, ensuring good convergence, such that the inclusion of more terms did not produce any significant change.

As in a previous work,[31] in order to simulate the experimental product translational energy distributions at the selected CM scattering angles reported in Refs. 22, 32, and 33, the recoil translational energy distribution at a selected CM scattering angle, $P(E_t'; \theta \pm \Delta\theta)$, was calculated using the equation

$$P(E_t'; \theta \pm \Delta\theta) = \sum_k N_k \exp\left[-\left(\frac{E_t' - E_k}{\Delta E_k}\right)^2\right] \times \int_{\theta-\Delta\theta}^{\theta+\Delta\theta}\left(\frac{1}{\sigma_R}\frac{d\sigma_R}{d\omega}\right)_k \sin\theta d\theta, \quad (7)$$

where the summation extends to every rovibrational state $k = (v', j')$ of the OH(OD) product, E_k is the D(H)-atom CM recoil energy corresponding to the OH(OD) internal state k, and $(d\sigma_R/d\omega)_k$ is the QCT v', j' state-resolved DCS.

The limited resolution of the experiment is modeled with a Gaussian centered at E_k, a normalization constant N_k, and ΔE_k given by

TABLE I. Present adiabatic and nonadiabatic QCT total integral reaction cross sections, σ_R, and intramolecular branching ratios, Γ(OD/OH) for both channels of the $O(^1D)$+HD reaction at 0.089 and 0.196 eV collision energies and a HD rotational temperature of 50 K (81% in $j=0$ and 19% in $j=1$). Values in parentheses correspond to one standard deviation of σ_R.

	PES	σ_{OH+D}/Å^2	σ_{OD+H}/Å^2	Γ(OD/OH)
E_{col}=0.089 eV				
	$1A'$ DK	7.24(3)	14.03(3)	1.94
E_{col}=0.196 eV				
	$1A'$ DK	6.28(2)	11.46(2)	1.82
	$1A''$ DK	0.669(4)	2.087(7)	3.12
	$2A'$ TSH DK	0.446(4)	0.928(6)	2.08
	$[1A', 2A']_{sh}+1A''$ DK	7.34(2)	14.48(2)	1.96
	$1A'$ K	6.94(1)	10.59(2)	1.53
	$1A''$ K	1.334(6)	2.259(7)	1.69
	$1A' + 1A''$ K	8.27(1)	12.85(2)	1.55

$$\Delta E_k = \frac{2m_C M}{m_{AB}} w_k \Delta w, \quad (8)$$

where $m_C = m_D$ and $m_{AB} = m_{OH}$ for the OH+D channel and $m_C = m_H$ and $m_{AB} = m_{OD}$ for the OD+H channel, and $M = m_O + m_{HD}$. The product recoil velocity resolution Δw is defined as

$$\Delta w = [\sin^2\theta\cos^2\phi(\Delta w_x)^2 + \sin^2\theta\sin^2\phi(\Delta w_y)^2 + \cos^2\theta(\Delta w_z)^2]^{1/2}, \quad (9)$$

where Δw_x, Δw_y and Δw_z are 750, 150, and 1100 m s^{-1}, respectively.[31]

The QCT calculations do not allow for the electronic fine structure states of the open shell OH/OD($^2\Pi$) radicals. Even if the spin-orbit and Λ-doublet levels were populated statistically by reaction, it is possible that the additional fine structure would modify and blur the experimentally derived $P(E_t', \theta)$ distributions relative to those calculated here *via* QCT methods. To check that this is not a significant problem, the theoretical $P(E_t', \theta)$ distributions have been recalculated using more accurate product v', j' energy levels which include approximately the fine structure splittings. The populations in the fine structure levels were assumed to be statistical, and the v', j' populations were taken from the QCT data. The resulting $P(E_t', \theta)$ distributions were found to be almost indistinguishable to those obtained directly from the QCT calculations neglecting the fine structure states of the products. Nevertheless, the simulations presented here were carried out using Eq. (7) with the k index running over rovibrational, spin-orbit and Λ-doublet levels of OH(OD).

III. RESULTS

A. Adiabatic calculations

The total integral reaction cross sections (i.e., the cross sections summed over the product quantum states) calculated adiabatically on the $1A'$ DK PES at 0.089 eV and on the two ($1A'$ and $1A''$) DK PESs at 0.196 eV, employing an HD rotational temperature of 50 K, are listed in Table I. At 0.089 eV, the contribution of the upper $1A''$ PES is negligible and no calculations employing it have been carried out. In general, the cross sections for the production of OD+H are no-

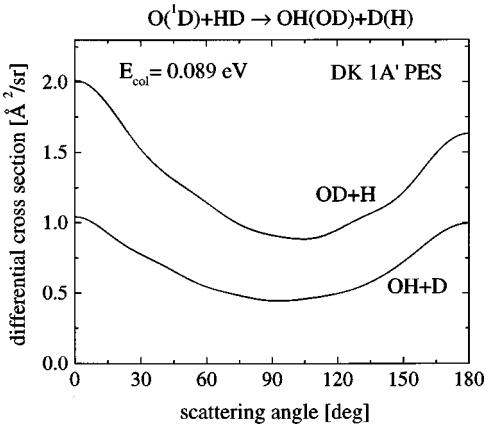

FIG. 1. QCT differential cross sections summed on final states for the OH+D and OD+H arrangement channels at 0.089 eV collision energy calculated on the ground $1A'$ DK PES.

tably larger than those for OH+D. The corresponding differential cross sections are shown in Figs. 1 and 2. For both exit channels, the DCSs calculated on the ground $1A'$ PES exhibit a broad minimum centered at a CM scattering angle of 90° with maxima at 0 and 180°. At both collision energies the DCS on the $1A'$ DK PES for the OH+D exit channel has approximately forward/backward symmetry, whereas that for the OD+H channel is slightly asymmetric, favoring forward scattering. In contrast, reactive scattering over the $1A''$ surface at $E_{col}=0.196$ eV (see Fig. 2) is restricted largely to the backward hemisphere for both OH and OD product channels.

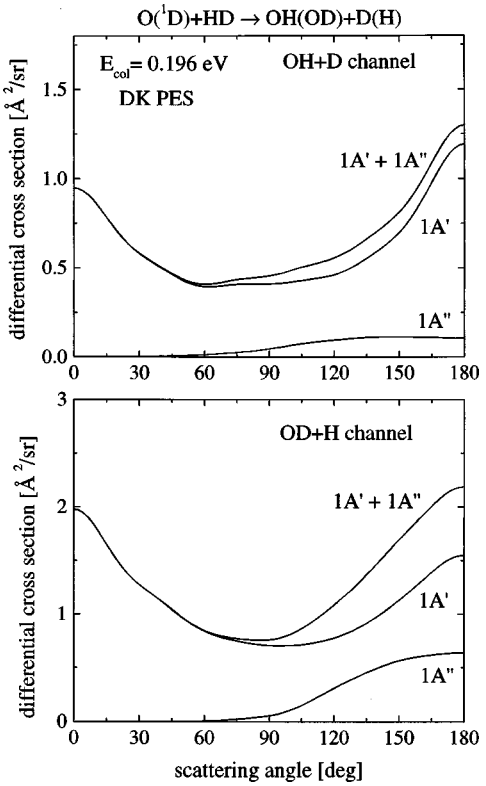

FIG. 2. QCT differential cross sections summed on final rovibrational states for the OH+D (upper panel) and OD+H (lower panel) arrangement channels at 0.196 eV collision energy. In each panel the joint and separate contributions of the $1A'$ and $1A''$ DK PESs to the DCSs are shown.

The DCSs have maxima at 180° and are nearly constant in the 150–180° angular range. The contribution from scattering over the $1A''$ surface therefore enhances the intensity of the DCS in the backward direction. The resulting total adiabatic DCS (i.e., that including the contributions from the $1A'$ and $1A''$ PESs) for the OH+D products is slightly backward asymmetric, while that for OD+H is nearly backward/forward symmetric. The ratio of the backward maximum to the sideways minimum is approximately 2.8 for the two isotopic reaction pathways.

Previous adiabatic QCT calculations at $E_{col}=0.196$ eV employing the K PESs,[31] under exactly the same conditions as those used here, lead to similar DCSs for the $1A'$ surface, but to a larger contribution from the $1A''$ PES, especially in the OH+D exit channel (the integral cross sections for which are also given in Table I). The angular distributions derived on the $1A''$ K PES are also more sharply peaked around 180° compared with those generated on the $1A''$ DK PES. While the cross section for sideways scattering determined on the $1A'$ K PES has approximately the same value as that on the DK PES, the enhanced backward scattering on the $1A''$ K PES leads to a deeper central minimum in the total $(1A'+1A'')$ adiabatic DCS. The ratio of the backward maximum to the sideways minimum for the K PESs is roughly 3.7 for the two isotopic channels.[31]

Experimental total DCSs for the title reaction at 0.089 and 0.196 eV collision energies have been reported by Liu and co-workers.[21,22,32,33] Although the results are generally in good agreement with the present calculations on the DK PESs, there are some interesting differences. At 0.196 eV collision energy, the experimental DCS for the production of OH+D is nearly backward/forward symmetric with a slight backward bias, whereas that for the generation of OD+H has a marked anisotropy, favoring the backward direction (see Figs. 17 and 18 of Ref. 33). The experimental total DCS[33] for the OH+D channel is in reasonably good agreement with the adiabatic DCS calculated on the K $(1A'+1A'')$ PES,[31] and with those presented here in Fig. 2, employing the DK PESs. For the OD+H channel, however, the clear preference for backward scattering observed experimentally is not evident in the QCT calculations employing either the K[31] or the DK PESs. In addition, one of the most pronounced differences between theory and experiment is found in the intensity ratio of the backward/forward peaks and sideways scattering, with the experimental quotients being appreciably larger than those derived theoretically in all cases.

Product vibrationally state-resolved DCSs for both OH and OD product channels at a collision energy of 0.196 eV are shown in Fig. 3. The DCSs for the $1A'$ DK PES at the lower collision energy, $E_{col}=0.089$ eV (not shown), are very similar to those obtained on the A' PES at 0.196 eV, except for the global factor of the cross section; all vibrationally state-resolved DCSs generated by reaction over the ground electronic state are approximately backward/forward symmetric. Note that the DCSs presented here at 0.196 eV, calculated on the $1A'$ DK PES, are very similar to those reported previously using the $1A'$ K version of the ground state PES.[31] At 0.196 eV, the QCT calculations predict the reaction dynamics on the excited $1A''$ DK PES to be very

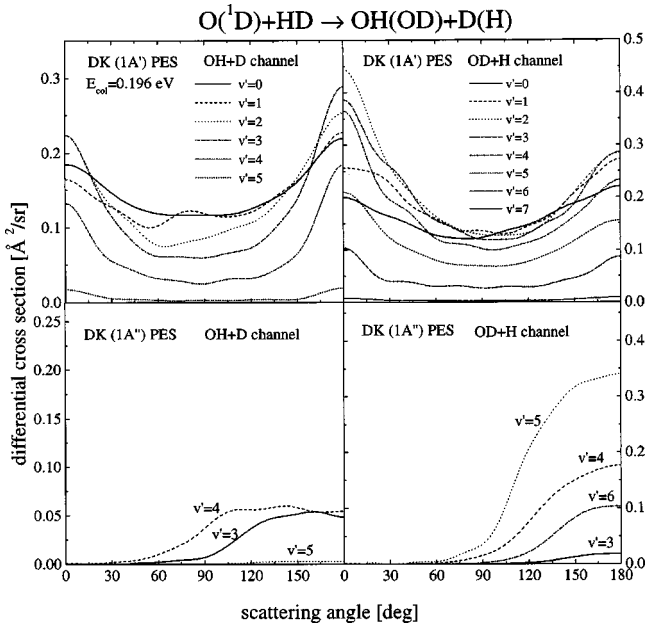

FIG. 3. Vibrationally state-resolved DCSs for the two channels of the $O(^1D)+HD$ reaction calculated adiabatically on the $1A'$ DK PES (top panels) and on the $1A''$ DK PES (bottom panels) at 0.196 eV collision energy.

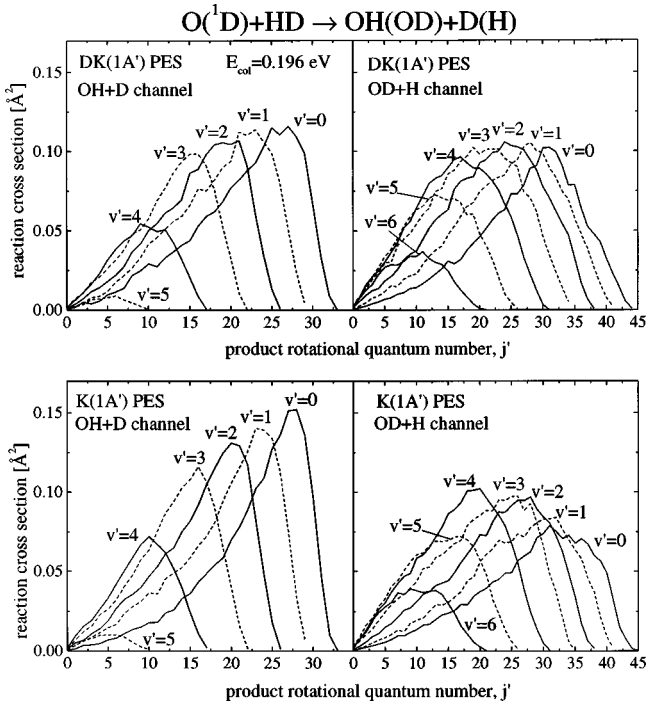

FIG. 4. Vibrationally state-resolved rotational distributions for both channels of the $O(^1D)+HD$ reaction calculated on the $1A'$ DK PES (top panels) and on the $1A'$ K PES (bottom panels) at 0.196 eV collision energy. Notice the slight population inversion obtained on both versions of the $1A'$ PES for the OD+H channel of the reaction.

different from that generated by reaction over the ground $1A'$ state surface, as clearly evident from the v' resolved DCSs shown in Fig. 3. The v' state-resolved DCSs corresponding to the $1A''$ DK surface are strongly backward peaked, as expected. For reaction on this PES, significant discrepancies are apparent between the DCSs derived from the DK and K[31] versions of the $1A''$ PESs: the angular distributions are always broader and the cross sections for the OH+D reactive channel are significantly lower on the DK PES. Furthermore, although both PESs yield a population inversion with a maximum at $v'=5$ in the OD+H channel, the relative occupancy of the various v' states is different. In particular, the DCS for the production of $v'=6$ is smaller than that for $v'=4$ over the whole angular range on the DK PES, and the cross section in the 160–180° interval is smaller by a factor of four than that calculated on the $1A''$ K PES.

The OH and OD rotationally resolved integral cross sections (ICS) for the reaction on the $1A'$ DK PES are depicted in the upper panels of Fig. 4. The corresponding j'-resolved ICSs calculated on the $1A'$ K surface[31] are shown for comparison in the lower panels of the figure. The two versions of the ground state potential yield v',j' distributions with similar shapes for both OH and OD product channels; for all the vibrational states populated, the rotational distributions are broad and extend to high values of j'. Both versions of the ground state surface predict somewhat different rovibrational distributions for the OH+D and OD+H channels. The distribution of vibrational states for OH+D is predicted to have a maximum at $v'=0$ on both the K and DK A' PESs, with monotonically decreasing populations with increasing v'; within each vibrational state, the rotational distributions are markedly asymmetric, with maxima closer to the higher j' end. For OD+H, the vibrational distributions show a population inversion on both surfaces, which is somewhat more marked for the K PES. Finally, the OD rotational distributions on the DK PES are more symmetric, i.e., somewhat less biased in favor of high j', than those obtained on the K PES.

The most dramatic discrepancy between the dynamics predicted by the alternative K and DK versions of the surfaces is found in the rotational state distributions generated by reaction over the A'' PES (see Fig. 5). Although the two excited state surfaces both yield OH and OD rotational distributions which are colder than those obtained on the ground electronic state, the distributions corresponding to the K A'' PESs (lower panels of Fig. 5) exhibit a remarkable bimodality, particularly in the OH + D reaction channel, that is not observed for reaction over the DK version of the A'' PES. The latter yields unimodal rotational distributions (upper panels of Fig. 5). As discussed in our previous article,[31] the bimodality obtained in the calculations on the $1A''$ K PES is indicative of the occurrence of two distinct dynamical mechanisms, the origin of which can be traced back to the particular topologies of the relevant PESs, as discussed in Sec. IV.

The effect of HD initial rotation ($j=0,1$) on reactivity over the $1A''$ PES is shown in Table II, where the total integral cross sections calculated on the K and DK PES at $E_{\mathrm{col}}=0.196$ eV are presented. Whereas the influence of rotation on the cross section is negligible on the $1A'$ PES, its effect on the reactivity on the $1A''$ surface is very considerable, especially for the OH+D reaction channel. Interestingly, while initial rotation from $j=0$ to $j=1$ enhances the reactiv-

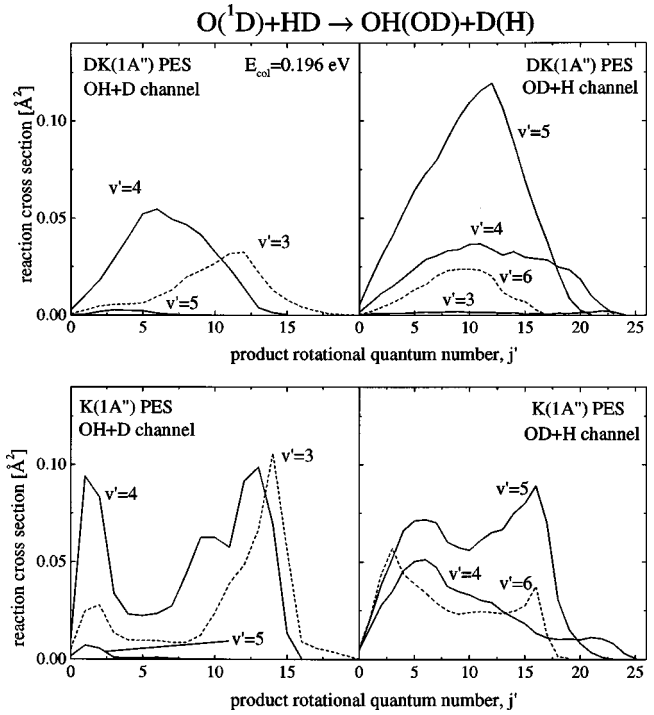

FIG. 5. Vibrationally state-resolved rotational distributions for both channels of the $O(^1D)+HD$ reaction calculated on the $1A''$ DK PES (top panels) and on the $1A''$ K PES (bottom panels) at 0.196 eV collision energy. Notice the population inversion and v' state-resolved unimodal rotational distributions obtained on the $1A''$ DK PES, in strong contrast with those obtained on the $1A''$ K PES showing a clear bimodality.

ity on the $1A''$ DK PES, the opposite effect takes place on the corresponding K PES. The reasons for this behavior will be examined in detail in Sec. IV.

B. Nonadiabatic calculations

The nonadiabatic calculations presented in this work have been performed using a TSH methodology which does not allow for hops at atom-diatom separations larger than 1.9 Å and, hence, in the asymptotic region where the two surfaces are degenerated. In addition, the probability of hopping is calculated with the Landau-Zener formula once the intersection between the two surfaces in the diabatic representation has been reached. By allowing hops in the asymptotic region, as it was done in Ref. 30, the reactivity assigned to the $2A'$ PES is going to be borrowed from that on the $1A'$ PES at collision energies below the $2A'$ barrier. Therefore, by using the TSH method of Ref. 30, the predicted reactivity on the $2A'$ PES will be larger at the expense of that on the $1A'$ PES. Moreover, the dynamics on the $2A'$ PES caused by transitions in the asymptotic region will be that of the $1A'$ PES and thus the net difference between the dynamics on the $1A'$ and the coupled $1A'/2A'$ will take place at energies above the $2A'$ barrier to access the region of the conical intersection.

TABLE II. Adiabatic QCT total integral reaction cross sections, σ_R, and intramolecular branching ratios, Γ(OD/OH), for both channels of the $O(^1D)+HD(j=0,1)$ reaction calculated on the $1A''$ K and DK PESs at $E_{col}=0.196$ eV.

PES	j	σ_{OH+D}/Å^2	σ_{OD+H}/Å^2	Γ(OD/OH)
$1A''$ DK	0	0.604	2.071	3.43
$1A''$ DK	1	0.942	2.154	2.29
$1A''$ K	0	1.462	2.347	1.61
$1A''$ K	1	0.776	1.881	2.42

Rigorously speaking, the contribution from each surface alone cannot be separated and what is really meaningful is the coupled dynamics on the $1A'/2A'$ surfaces. However, in the following we will show results of integral and differential cross sections obtained by using the present TSH method with trajectories starting on the $2A'$ surface to show the dynamics arising from nonadiabatic transitions in the region of the conical intersection. Integral and differential cross sections corresponding to the present TSH calculations starting on the ground $1A'$ PES are almost indistinguishable from those obtained in the adiabatic QCT calculations performed on the $1A'$ PES, and, therefore, they will not be considered further.

The total integral TSH cross sections corresponding to trajectories starting on the $2A'$ DK surface calculated at $E_{col}=0.196$ eV are listed in Table I. As can be seen, the $2A'$ cross section for the production of OD+H is a factor of two larger than that for the production of OH+D. Note that these cross sections are sensibly smaller than the corresponding ones obtained in the adiabatic calculations on the excited $1A''$ PES (by about 66% for the OH+D channel and by 44% for the OD+H channel). Interestingly, the intramolecular branching ratio, Γ(OD/OH), obtained by considering the contributions of all the $1A'$, $2A'$ and $1A''$ DK PESs is 1.96 at $E_{col}=0.196$ eV (see Table I). This value is somewhat larger than the experimental value of 1.73 obtained by Liu and co-workers.[42] The QCT Γ(OD/OH) obtained from the adiabatic calculations on the ground $1A'$ DK PES is 1.82 and the corresponding values obtained on the $1A'$ K and on the $1A'+1A''$ K PESs are 1.53 and 1.55, respectively. Therefore, no definitive conclusion can be obtained about the participation of the excited $1A''$ and $2A'$ surfaces on the reactivity of the title reaction from the intramolecular branching ratio data.

The TSH differential cross sections (both total and product vibrational state-resolved) are shown in Fig. 6. Reactive scattering extends over the whole angular range in both exit channels, but the angular distributions are quite different. The total DCS for the OH+D channel has a prominent forward peak, while, in contrast, that for the OD+H channel shows a pronounced backward maximum. These features are also present in the respective v' resolved DCSs. In the two isotopic channels, the vibrational distributions are inverted, but to a lesser extent than the inversion generated by reaction over the $1A''$ surface. The maxima for the OH+D and OD+H channels are found at $v'=4$ and $v'=5$, respectively.

Figure 7 shows the contributions to the reactive DCSs from the three surfaces under consideration, as well as the total DCS including the coupled dynamics on the $1A'$ and $2A'$ surfaces and the contribution from the $1A''$ PES. The calculated nonadiabatic cross sections are found to contribute less than 10% to the total reactivity (see Fig. 7 and Table I), and have a small influence on the overall shape of the total

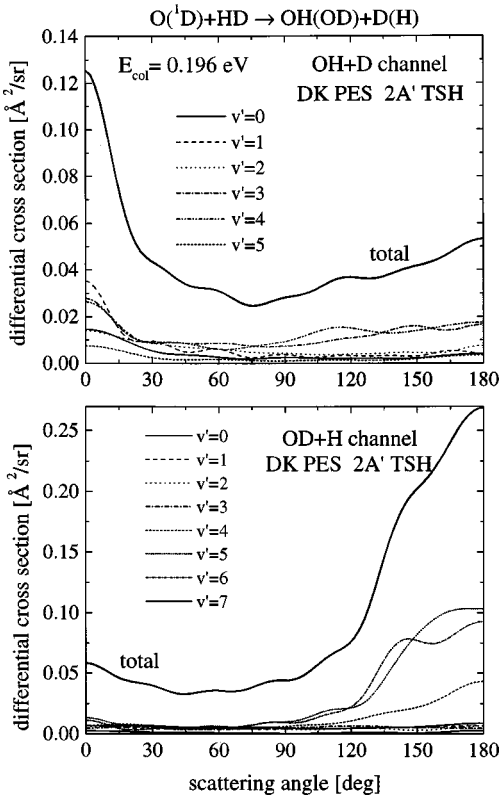

FIG. 6. Total and vibrationally state-resolved differential cross sections calculated using the TSH methodology starting trajectories on the $2A'$ DK PES for both channels of the $O(^1D)+HD$ reaction at 0.196 eV collision energy. Recall that these DCSs represent the dynamics due to hops at the crossing seam (see text for more details).

DCSs. The $2A'$ state is not available in the K version of the potential surface, but nonadiabatic calculations using TSH methods[8,13] have been reported for $O(^1D)+H_2$ on DIM PESs developed by Kuntz *et al.*[7] The DIM value for the $2A'$ collinear barrier is about 0.16 eV (as compared to the $\approx$0.10 eV barrier on the $2A'$ DK surface). Schatz *et al.*[13] have reported TSH calculations on the three relevant DIM surfaces for a collision energy of 0.22 eV, not too far from the value of 0.196 eV used here. Although comparison between the DIM results and the present calculations can only be approximate (not least because they refer to different isotopic variants), it is worth noting that the most salient qualitative features of the nonadiabatic calculations on the DIM surfaces are similar to those reported here on the DK PESs. As with the present calculations, the DIM PES calculations lead to a relatively small cross section (about half that associated with the $1A''$ PES), which has little influence on the total cross section, either integral or differential. Reactive scattering from DIM $2A'$ PES is distributed over the whole angular range, but the distribution is nearly isotropic, without the peaks in the forward or backward directions that are found here in both exit channels of the $O(^1D)+HD$ reaction on the DK PES. Finally, in common with the present calculations, the vibrational state distributions obtained by Schatz *et al.*[13] on the $2A'$ DIM PES have a slight population inversion, i.e., the distributions are intermediate in character between those derived *via* adiabatic calculations on the $1A'$ and $1A''$ surfaces.

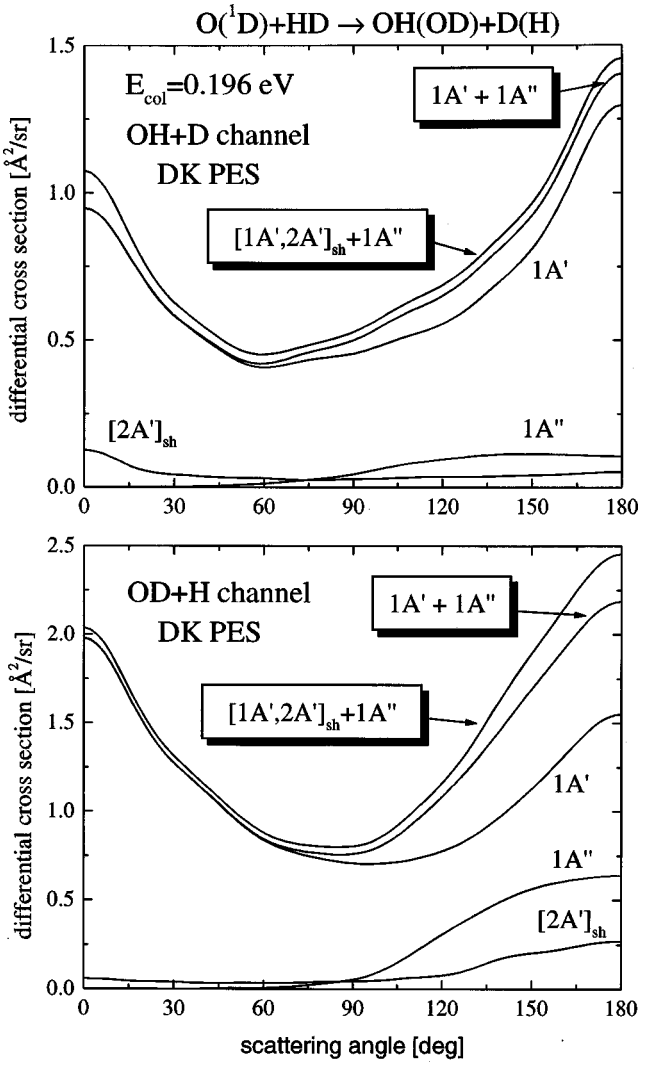

FIG. 7. Total differential cross sections calculated on the three surfaces under consideration $1A'$, $1A''$ and $2A'$, as well as the total DCS, including the coupled dynamics on the $1A'$ and $2A'$ surfaces and the contribution from the $1A''$ PES for both channels of the title reaction at 0.196 eV collision energy.

C. Simulation of experimental results

The results of the present calculations on the DK PESs are compared with the recent measurements by Liu and co-workers[32,33] for the two isotopic exit channels of the title reaction in Figs. 8–13. The experimentally derived product translational energy distributions have been simulated by transforming and folding the QCT calculated rovibrationally state selected DCSs with the reported experimental spread in angles and velocities, as described in Sec. II. The QCT simulations shown in Figs. 8–13 allow for the splittings of the OH(OD) internal states into spin-orbit and Λ-doublet components, although as noted in Sec. II, at the resolution of the experiment the blurring effect of this fine structure is very small. For the lower collision energy (E_{col}=0.089 eV), the simulations are based on the adiabatic calculations on the $1A'$ DK PES, since at this collision energy the contribution to reaction from the excited PESs is negligible, whereas at E_{col}=0.196 eV the adiabatic and nonadiabatic calculations on the $1A'$, $1A''$ and $2A'$ have been considered.

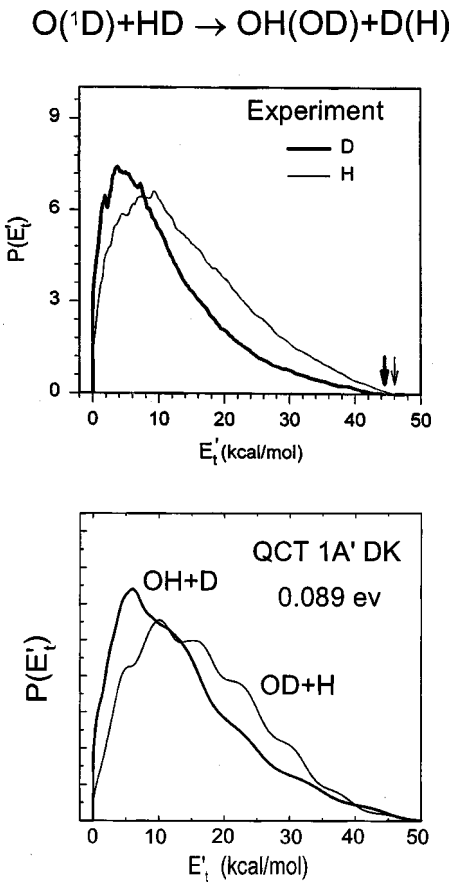

FIG. 8. Total OH (thick curve) and OD (thin curve) product translational energy distributions, $P(E_t')$, at 0.089 eV collision energy. Top panel: experimental results from Ref. 32. Bottom panel: simulation from the QCT results on the $1A'$ DK PES.

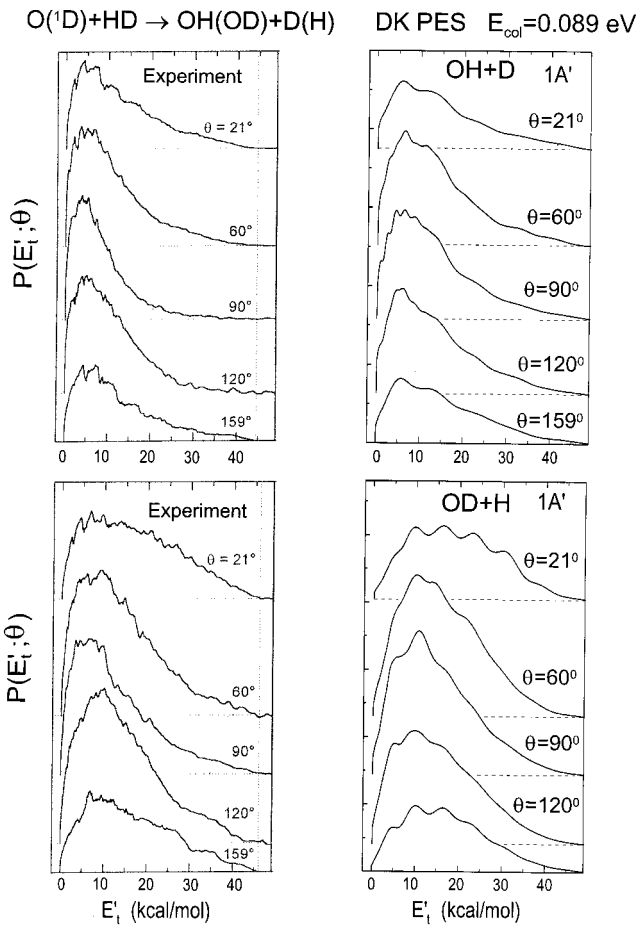

FIG. 9. Products' translational energy distributions at selected CM scattering angles, $P(E_t', \theta, \Delta\theta = 3°)$, of the OH product at 0.089 eV collision energy. Left panels: experimental results from Ref. 32 for the OH + D (top) and OD + H (bottom) channels. Right panels: Simulations from the QCT results on the $1A'$ DK PES.

The comparison of the experimental and simulated total (i.e., integrated over all scattering angles) product translational energy distribution, $P(E_t')$, at $E_{\mathrm{col}}=0.089$ eV for the two exit channels are represented in Fig. 8. The agreement is fairly good, except for the fact that the theoretical distributions are somewhat broader than the experimental ones. Figure 9 depicts the CM scattering angle resolved product translational energy distributions, $P(E_t', \theta \pm 3°)$ obtained experimentally, together with the corresponding theoretical simulations. The overall agreement between theory and experiment is good and the main differences are found in the width of the distributions which, in general, are broader in the simulations, particularly in the case of $\theta=90°$ for the OH+D channel.

In an attempt to clarify the influence of the excited state PESs on the kinetic energy release distributions at the higher collision energy (0.196 eV), two types of simulations were performed; in the first only data from calculations on the ground state $1A'$ surface were used, while in the second both adiabatic and nonadiabatic contributions from the excited PESs were also included. The total $P(E_t')$ distributions for the OH+D and OD+H exit channels are shown in Figs. 10 and 11, respectively. As for the lower collision energy, the experimental distributions corresponding to both the OH+D and OD+H channels are somewhat narrower than the theoretical predictions using the $1A'$ PES alone. The structure around the peak maximum in the experimental distribution for the OH+D channel (Fig. 10) seems to be better reproduced by the simulation using just the data obtained on the ground state $1A'$ surface. The experimental distribution for the OD+H channel shows a pronounced unstructured peak that is somewhat better accounted for, however, by the simulations including the data from the ground and excited PESs, although the calculated $P(E_t')$ distribution exhibits undulations which are not seen experimentally. Overall, however, it would seem that a *smaller* contribution to reaction from the $1A''$ surface than predicted by the DK PES would yield distributions in better accordance with experiment.

The translational energy distributions for selected scattering angles are shown in Figs. 12 and 13. Here, once more, simulations are presented for both exit channels, employing either the QCT data on the ground $1A'$ state surface alone, or that derived when all relevant PESs were included. As expected, both theory and experiment yield better resolved signals for the reaction leading to OH+D, where the spacing of the internal molecular levels is wider. The influence of the $1A''$ surface is restricted to the backward hemisphere and, in fact, for both channels, the simulations on the ground state surface and those including the upper PESs are virtually indistinguishable for scattering angles lower than 90°.

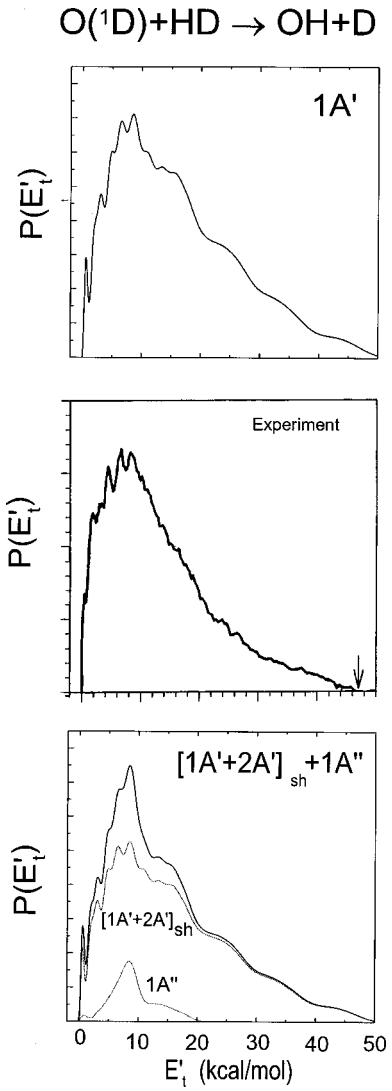

FIG. 10. Total OH product translational energy distribution, $P(E_t')$, at 0.196 eV collision energy. Middle panel: experimental results from Ref. 33. Top panel: simulation from the QCT results on the $1A'$ DK PES. Bottom panel: simulation from the QCT results on the $[1A'+2A']_{sh}+1A''$ DK PESs. The dotted traces of the bottom panel show the separated contributions from the $[1A'+2A']_{sh}$ and $1A''$ DK PESs as indicated.

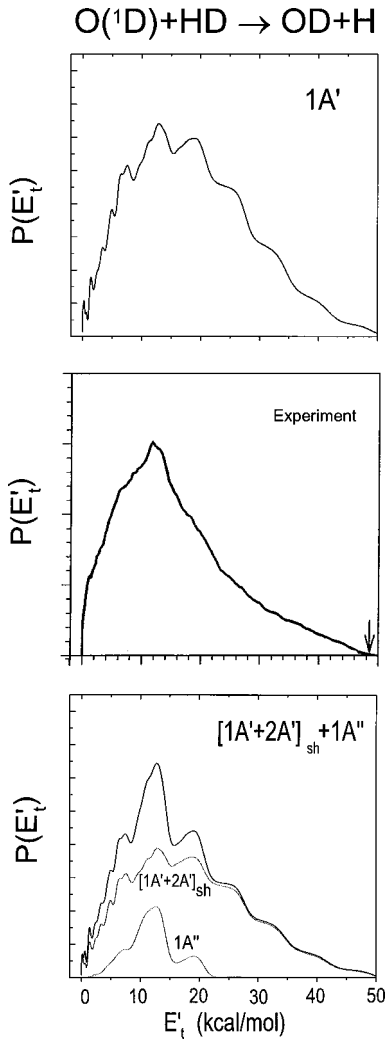

FIG. 11. Total OD product translational energy distribution, $P(E_t')$, at 0.196 eV collision energy. Middle panel: experimental results from Ref. 33. Top panel: simulation from the QCT results on the $1A'$ DK PES. Bottom panel: simulation from the QCT results on the $[1A'+2A']_{sh}+1A''$ DK PESs. The dotted traces of the bottom panel show the separated contributions from the $[1A'+2A']_{sh}$ and $1A''$ DK PESs as indicated.

For the OH+D channel (Fig. 12), the experimental $P(E_t';\theta)$ at 90 and 120° show pronounced structures around the maximum that are better reproduced by the simulations on the $1A'$ surface than by those including the upper PESs. As discussed previously,[31] the structure does not correspond to single rovibrational states, but rather to groups of rotational states (usually three), each of them from one of the lowest vibrational states $v'=0$, 1 and 2 of the OH molecule. For the higher v', the rotational states populated are lower, and they overlap more in energy, with the result that no clear structure can be identified. It must be emphasized that the observed structures *cannot* be associated with reaction over the $1A''$ PES. Toward 0 and 180°, the experimental resolution deteriorates and the peaks get gradually blurred. At 21 and at 159°, the experiment yields broad distributions which are approximately reproduced, both by the calculations on the $1A'$ PES and by those including all the three PESs. However, at 60° the theoretical simulations give clear structure which is not found experimentally. (The seemingly poorer experimental resolution at this scattering angle is not easily understood, since the resolution should be the same at 60 and 120°.) As with the simulations performed using the K PES, reported in Ref. 31, the clearest influence of the $1A''$ PES on the $P(E_t';\theta)$ is the contribution to the peak appearing at $E_t' \approx 10$ kcal mol^{-1}, which is much less pronounced in the experiment compared with the QCT calculations on the K PESs. The peak is even more pronounced in the present simulations employing the DK PESs: it would seem that the shapes of the experimental $P(E_t';\theta)$ distributions are best reproduced by the simulations which only allow reaction over the ground $1A'$ PES. The results indicate that the contribution of the $1A''$ PES to the reaction to give OH+D must be smaller than that predicted by the calculations on the DK PES.

The experiments of Liu and co-workers[33] yield broad kinetic energy release distributions for the OD+H channel, with different shapes at different CM scattering angles, but

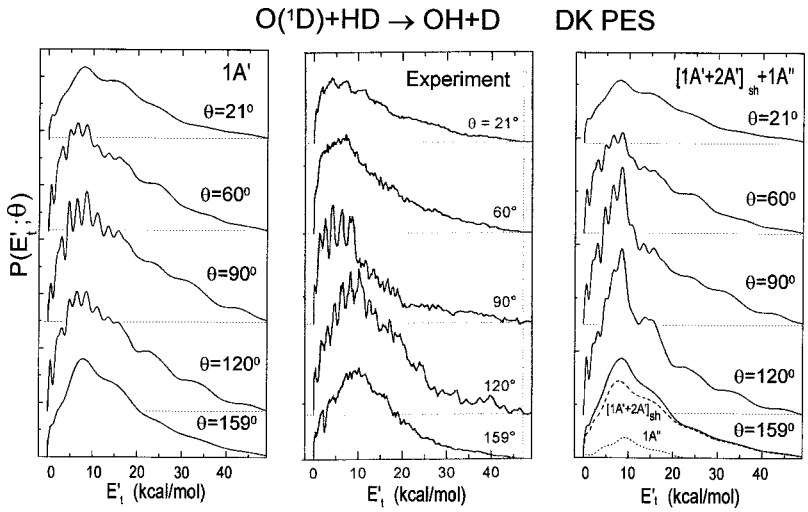

FIG. 12. Products' translational energy distributions at selected CM scattering angles, $P(E_t',\theta,\Delta\theta=3°)$, of the OH product at 0.196 eV collision energy. Middle panel: experimental results from Ref. 33. Left panel: Simulation from the QCT results on the $1A'$ DK PES. Right panel: Simulation from the QCT results on the $[1A'+2A']_{sh}+1A''$ DK PESs. The bottom traces of the right panel show the separated contributions from the $[1A'+2A']_{sh}$ and $1A''$ DK PESs as dashed and dotted curves, respectively.

without superimposed resolved peak structure. Except at 90° and product translational energies E_t' lower than 10 kcal mol^{-1}, where the QCT calculations show some structure, the resolution of the simulated distributions is comparable to that of the experiments. Once again, the backward scattered region is the one most sensitive to the participation of the $1A''$ excited state surface. In contrast to the results for the OH+D channel, the experimental distributions for the OD+H channel at 120 and 159° bear the closest resemblance to the simulations which *include* contributions from all the relevant PESs. In particular, the prominent experimental peak at $E_t'\approx 13$ kcal mol^{-1} is observed only in the multisurface simulation, where the peak intensity is overestimated. An analysis of the theoretical data shows that this peak is mostly attributable to scattering on the $1A''$ PES into the $v'=5$ level of the OD molecule. The two lower peaks on both sides of the theoretical maximum correspond to $v'=4$ and $v'=6$, respectively.

The clearest evidence for the involvement of the A″ excited state is observed, therefore, in the OD+H channel, and no significant excited state participation is evident from the experimental OH+D distributions, which, as shown above, are closer in shape to those simulated employing just the $1A'$ surface. Although the contribution from the A″ DK PES is predicted to be much lower in the OH+D channel compared with the OD+H channel, in agreement with the experimental evidence, the overall contribution from the A″ excited surface predicted by the QCT calculations seems to be too high. Better agreement between theory and experiment would result from a smaller contribution of the $1A''$ surface for both the OH and OD channels, which might be achieved, for example, by increasing the height of the barrier on the DK $1A''$ PES. The effect of reduced reactivity on the A″ PES would be to lower the height of the maxima in the simulated $P(E_t';\theta)$ distributions at selected angles in the backward hemisphere. In particular, the simulated kinetic energy release distributions for the OH+D channel employing all relevant PESs would become very similar to those generated using only the $1A'$ PES and, at the same time, lead to a decrease in the prominent peak in the $P(E_t';\theta)$ distribution at 120° in both the OH+D and OD+H channels, and a blurring of the three-maxima structure in the $P(E_t';\theta)$ for the OD+H channel at 159°. All of these effects would bring the simulations into better agreement with experiment.

Previously, we presented simulations based on QCT calculations on the $1A'$ and $1A''$ K PESs for the reaction yielding OH+D,[31] since at the time of publication experimental

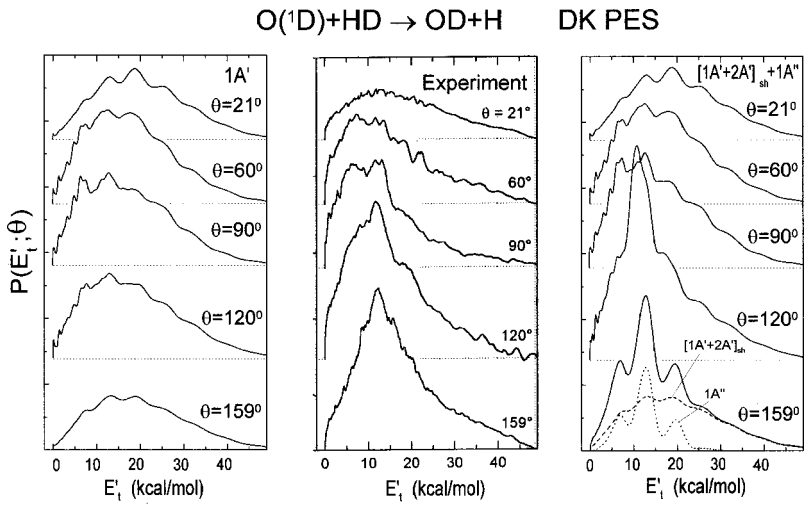

FIG. 13. Products' translational energy distributions at selected CM scattering angles, $P(E_t',\theta,\Delta\theta=3°)$, of the OD product at 0.196 eV collision energy. Middle panel: experimental results from Ref. 33. Left panel: Simulation from the QCT results on the $1A'$ DK PES. Right panel: Simulation from the QCT results on the $[1A'+2A']_{sh}+1A''$ DK PESs. The bottom traces of the right panel show the separated contributions from the $[1A'+2A']_{sh}$ and $1A''$ DK PESs as dashed and dotted curves, respectively.

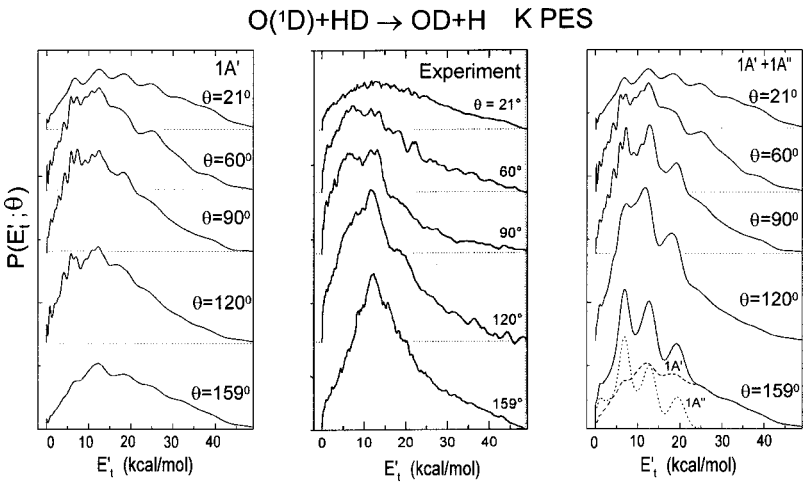

FIG. 14. Products' translational energy distributions at selected CM scattering angles, $P(E_t',\theta,\Delta\theta=3°)$, of the OD product at 0.196 eV collision energy. Middle panel: experimental results from Ref. 33. Left panel: Simulation from the QCT results on the $1A'$ K PES. Right panel: Simulation from the QCT results on the $1A'+1A''$ K PESs. The bottom traces of the right panel show the separated contributions from the $1A'$ and $1A''$ K PESs as dashed and dotted curves, respectively.

data were only available for that channel. It is of interest to see how the K PES performs in reproducing the experimental distributions for the OD+H channel reported in Ref. 33. Figure 14 shows the same kind of simulations for the OD+H channel as those presented in Fig. 13, but based on the adiabatic QCT calculations on the $1A'$ and $1A''$ K PESs. As in the case of the DK PES, the best agreement with experiment is obtained when the contributions from both the $1A'$ and $1A''$ PESs are considered (right panels). In fact, the agreement between theory and experiment at $\theta=90°$, and to a lesser extent at $\theta=120°$, is good. However, at $\theta=159°$, where the $1A''$ PES contributes most, the theoretical simulation shows a three-peak structure, which is most intense at $E_t'\approx 7$ kcal mol^{-1}. This structure is clearly at variance with experiment, and with the simulations based on the calculations on the DK PES (right panel of Fig. 13), where the maximum appears at $E_t'\approx 12$ kcal mol^{-1}. The characteristic three-peak structure in the simulation shown at the bottom of Fig. 14 has its origin in the bimodal rotational distributions for the OD products born in vibrational levels $v'=5$ and $v'=6$ predicted by the QCT calculations on the $1A''$ K PES (see Fig. 5). The present results suggest that the bimodality in the rotational distributions generated on the K version of the A″ PES is inconsistent with the experimental data of Liu and co-workers.[33]

IV. DISCUSSION

One of the most interesting findings of the present work has been the significant differences in reactivity between the adiabatic calculations on the K and DK versions of the $1A''$ PES. Specifically, the major discrepancies consist of: (a) the effect of initial rotation on the total cross sections, especially for the OH+D channel (see Table II); (b) the product rotational distributions predicted by the two versions of the $1A''$ PES (see Fig. 5). The consequences of this different dynamical behavior are relevant for the simulation of the experimental results. As commented on above, Lee and Liu[34] measured the excitation functions for the reaction of O(^1D) with p-H_2 (86% $j=0$) and n-H_2 (75% $j=1$) and they showed that at collision energies where the $1A''$ PES starts to contribute (above $\approx$0.09 eV), the reactivity for initial $j=1$ is larger than that for $j=0$. With regard to the product rotational distributions, it becomes apparent from the results displayed in Fig. 12 of the present work and in Fig. 5 of Ref. 31 for the OH+D channel, and in Figs. 13 and 14 of the present work for the OD+H channel, that the bimodal distributions predicted by the K PES, which give rise to the particular peak structure in the $P(E_t';\theta)$ for backward scattering angles shown in Fig. 14, are inconsistent with the experimental data (see Sec. III C).

It might at first be thought that the dynamical differences noted above must be a consequence of differences in the topologies of the reactant valleys of the two versions of the $1A''$ surface. However, the K and DK $1A''$ PES have almost indistinguishable minimum energy paths and bending potentials in the transition state region. The location and height of the transition state of the K and DK $1A''$ PES are almost identical (see Table III). Furthermore, as shown in Fig. 15, the $R-\gamma$ plots of the entrance channels of both PESs are barely distinguishable, apart from the slightly greater curvature of the potential contours on the K surface.

A detailed study of the influence of the initial angle of attack on reactivity shows that no migration takes place in the course of the approach of rotationless reagents on either of the two PESs; that is, O(^1D) atoms approaching the D(H) end of the HD molecule yield OD(OH) if reaction takes place. However, the cone of acceptance for the formation of OH is somewhat larger on the K PES than on the DK PES ($\gamma\in[120,180]$ on the former vs $\gamma\in[140,180]$ on the latter), whereas it is very similar for the reaction yielding OD. The larger cone of acceptance on the K surface thus explains why the reactivity for initial $j=0$ is larger; nevertheless, the plots of Fig. 15 do not provide a clear hint as to the origin of these different cones of acceptance. Two reactive trajectories for rotationless HD, labeled A and B, have been represented on

TABLE III. Properties of the collinear saddle points of the fits of the $1A''$ K and DK PESs: barrier height ($V^{\ddagger}$), internuclear distances ($r_{OH}^{\ddagger}$, $r_{HD}^{\ddagger}$) and imaginary and bending frequencies ($h\nu_i$ and $h\nu_{bend}$).

PES	$V^{\ddagger}$ (kcal/mol)	$r_{OH}^{\ddagger}$ (Å)	$r_{HD}^{\ddagger}$ (Å)	$h\nu_i$ (cm^{-1})	$h\nu_{bend}$ (cm^{-1})
K	2.3067	1.6286	0.7729	606*i*	339
DK	2.3211	1.6328	0.7702	660*i*	266

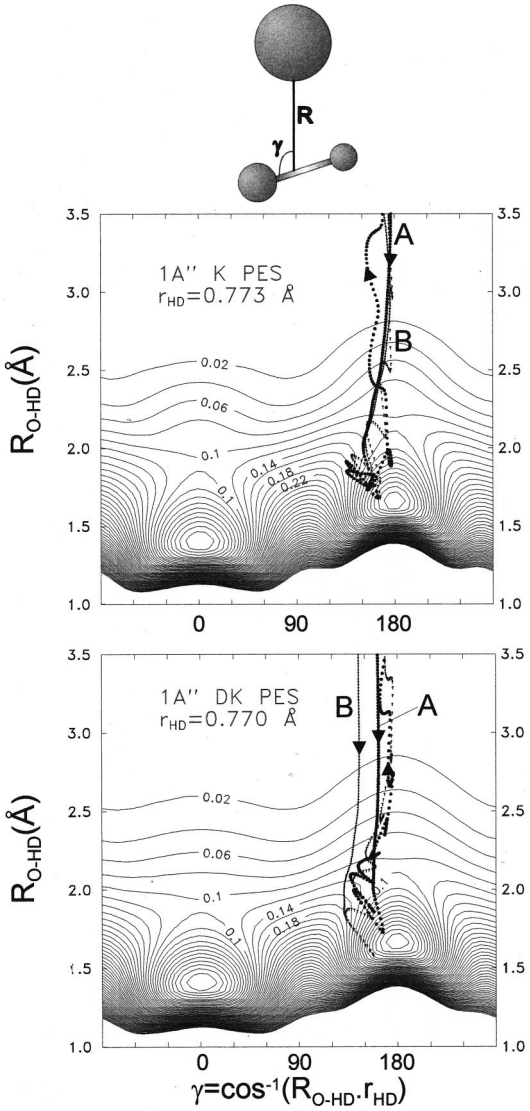

FIG. 15. Contour plot in entrance channel Jacobi $R-\gamma$ coordinates (see the top part of the figure for a definition) at the fixed HD internuclear distance corresponding to the saddle point of each PES. Top: $1A''$ K PES. Bottom: $1A''$ DK PES. Contours in eV. Two different characteristic trajectories, labeled A and B, attacking the H side of the molecule and yielding OH+D are represented in each PES. Trajectories A and B have the same initial conditions on the two PESs.

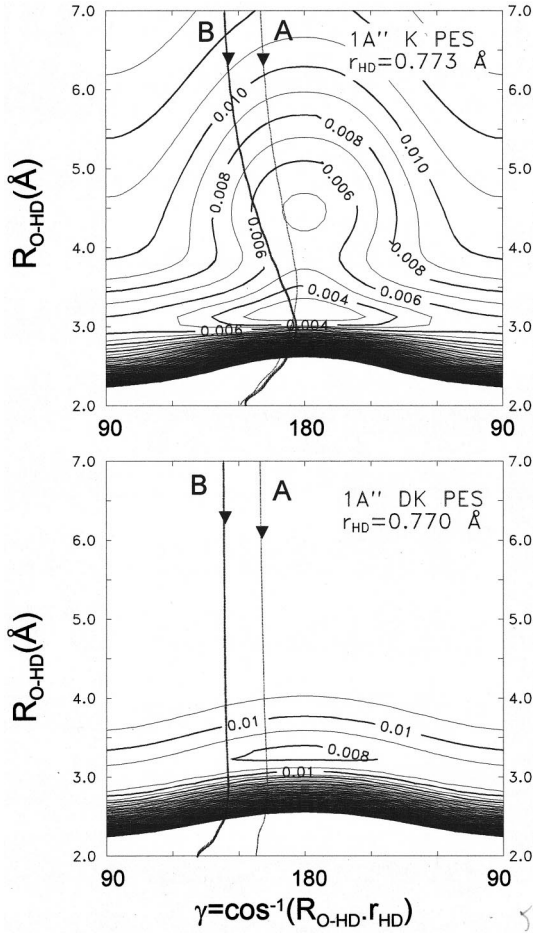

FIG. 16. Expanded view of the long range entrance channel plotted in $R-\gamma$ Jacobi coordinates displaying the H side of the molecule (90–180°). The contours are in intervals of 1 meV. Top: $1A''$ K PES. Bottom: $1A''$ DK PES. Trajectories A and B are the same as in Fig. 15. Notice that the shallow well at $R\approx 4.4$ Å and $\gamma=180°$ on the K PES is pulling both trajectories, deviating them from a straight line and causing a remarkable orientational effect.

the two PESs, in such a way that the A(B) trajectory has been run with identical initial conditions on the two surfaces. In spite of the identical starting conditions, a close inspection of the trajectories reveals that already at an R distance of 3.5 Å, trajectory B (and to a less extent trajectory A) is different on the two PESs. Clearly, to explain this requires following the trajectories from larger R, and a careful examination of the long range topology of the surfaces. Figure 16 depicts the R-γ plots at R distances up to 7 Å plotting potential contours at intervals of 1 meV. On the DK PES, at distances in excess of 4 Å, the potential is nearly zero and the two trajectories approach the interaction region in a straight line. However, on the K surface the existence of long range features, in particular a shallow well at $\gamma=180°$ and $R\approx 4.5$ Å, causes trajectories to be oriented toward the collinear configuration, and, as a result, the trajectories follow a curved pathway. It is the existence of these subtle features on the A″ K PES which is the origin of the larger cone of acceptance and therefore the larger reactivity at $j=0$ in comparison with the DK PES. For reaction with HD($j=1$), the torques produced by these contours on the K PES are negligible with respect to rotation and the consequence is a decrease of reactivity when j increases. On the other hand, it is expected that in the absence of orientational effects, as is the case of the DK PES, rotation will promote reaction to yield OH+D, as observed previously for other collinear reactions (see, for example, Ref. 43).

The existence of the long range features on the $1A''$ K PES is likely to be an artifact of the fitting procedure since no *ab initio* points were calculated at such long distances.[11] It should be noted that a quantum mechanical scattering calculation would be much less sensitive to the ''orientational effects'' caused by these long range artifacts on the K surface. In fact, preliminary QM calculations[44] on the $1A''$ K PES yield a cross section for the $O(^1D)+HD(j=0)\rightarrow OH+D$ reaction closer to that obtained in QCT calculations for the reaction with HD($j=1$) on the same surface.

The OH and OD product rotational distributions predicted by the QCT calculations on the K and DK A″ excited state surfaces are so different (see Fig. 5) that some remarks concerning the origin of the bimodal rotational distribution generated on the K PES are warranted. In spite of the different topology found in the long range entrance valley of the two A'' surfaces, a detailed study of the ensemble of reactive trajectories shows that the bimodal rotational distribution generated on the K A'' PES is *uncorrelated* with properties of the entrance channel, such as impact parameter or angle of attack. Therefore, one is forced to the conclusion that it is differences in the exit channels which account for the different behavior of the K and DK A'' PES. To highlight the role of the exit channel, Fig. 17 shows contour plots of the OH+D exit channel of the two A″ potentials, in the form of an R'-γ' diagram analogous to those shown above for the entrance channel. The very high curvature of the contours on the plot for the K A″ PES, relative to that on the DK PES, is now clear to see. Superimposed on the contour plots for each surface are the same trajectories A and B already shown in Figs. 15 and 16, but now plotted as a function of the OH+D exit channel Jacobi coordinates. Notice that in this coordinate system, only the exit part of each trajectory is meaningful. On the DK PES, both trajectories give OH($v'=4$) in $j'=8$, the most populated OH product state. On the K PES, on the other hand, the two trajectories part company early in the exit channel, with trajectory A yielding OH in ($v'=4, j'=12$) and trajectory B yielding OH in ($v'=4, j'=2$). On the K PES, the sharply varying contours with R' and γ' lead to a bifurcation in the trajectories into two groups, one leading to low rotation (where the reaction remains essentially collinear from reactants to products), and the other leading to high rotation. On the more smoothly varying DK A'' PES there is essentially just one class of trajectory, i.e., that which leads to rotational excitation intermediate between the two extreme limits observed on the K PES. Since the experimental evidence is against the existence of bimodal rotational distributions, it must be concluded that the DK version of the A'' is more accurate in representing the exit valley than the K PES. Preliminary QM calculations confirm the QCT results with respect to the rotational distributions found on the two versions of this electronically excited PES.[44]

A final issue to be addressed is the importance of nonadiabatic effects. As shown above, QCT-TSH calculations indicate that nonadiabatic effects are of minor importance for the overall description of the dynamics of the title reaction at $E_{col} \leqslant 0.2$ eV. The total reactivity on the $2A'$ is to a large extent governed by the entrance barrier, which it has in common with the $1A''$ PES: the final state distribution is, however, quite different from that generated on the $1A''$ surface. The opacity functions (not shown) provide some hints to help explain the different DCSs found for the two isotopic channels (see Fig. 6). The reaction probability is much larger for the reaction producing OD+H than that yielding OH molecules up to impact parameters of about 1.35 Å (orbital angular momenta, $l \approx 20$). However, beyond these impact parameters, the reaction yielding OH+D is favored. This would explain the presence of the forward peak in the

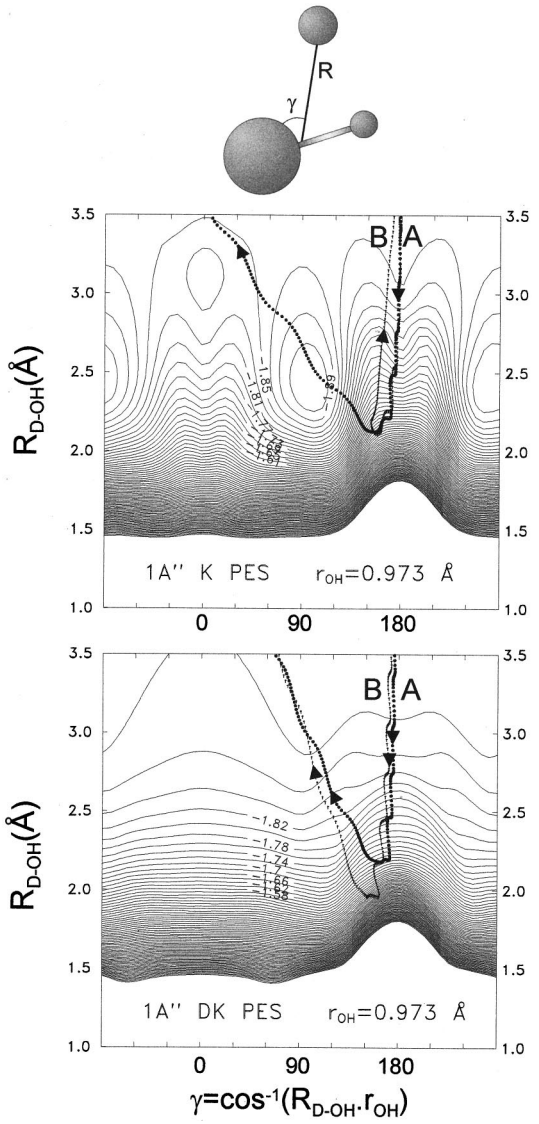

FIG. 17. $1A''$ $R'-\gamma'$ contour plots of the exit OH + D channel in Jacobi coordinates (see the top part of the figure for a definition) at the equilibrium internuclear distance of the OH molecule. Trajectories A and B are the same as those in Figs.15 and 16. Whereas on the K PES (top) trajectory A gives rise to a high rotational excitation ($j'=12$) and trajectory B to a low rotational excitation ($j'=2$), on the DK PES (bottom) both trajectories produce OH in $j'=8$. Notice that in both cases trajectories A and B tend to follow the direction of steepest descent. Contours in eV with the origin of energy taken in the asymptotic O(^1D)+HD reactant valley at the equilibrium distance of the HD molecule.

OH+D DCS. In contrast with the reaction on the $1A''$ surface, about 12% of the reactive trajectories are migratory for both reactive channels on the $2A'$ PES. Whereas the maximum impact parameter for nonmigratory trajectories producing OD+H is ≈1.4 Å, that for migratory trajectories is ≈1.7 Å. The opposite occurs for the OH+D channel; that is, $b_{max} \approx 1.8$ Å for nonmigratory trajectories whereas $b_{max} \approx 1.4$ Å for migratory trajectories. Interestingly, while there exists a strong correlation between impact parameter and scattering angle for nonmigratory trajectories, this correlation is practically absent for the migratory ones and, in addition, the latter generally have longer collision times than the former.

V. SUMMARY AND CONCLUSIONS

Detailed adiabatic and nonadiabatic QCT calculations have been performed of the $O(^1D)+HD$ reaction employing the new *ab initio* versions of the $1A'$, $1A''$ and $2A'$ potential energy surfaces of Dobbyn and Knowles.[26] Integral and differential cross sections for both the OH+D and OD+H exit channels have been determined at 0.089 and 0.196 eV collision energies. The results have been compared with other calculations using different potential energy surfaces and have been used to simulate the experimental product translational energy distributions determined in recent molecular beam experiments by Liu and co-workers.[32,33]

The comparison between the experimental results and the theoretical simulations reveals for the OH+D channel a better agreement when only the $1A'$ surface is considered in the dynamical calculations, whereas for the OD+H channel, it seems that the contribution of the excited $1A''$ surface is necessary to account for the experimental results. In general, a smaller participation from the excited A″ state than that predicted by the QCT calculations on the DK PESs would lead to better agreement between experiment and theory.

The main differences between the adiabatic calculations on the DK and K PESs occur for the excited $1A''$ state: the two alternative A″ surfaces yield dynamical features which should be clearly distinguishable experimentally. In particular, the effect of reagent rotation (from $j=0$ to $j=1$) on reactivity has been found to be opposite in the QCT calculations on the K and DK $1A''$ PESs. In addition, distinctly bimodal product rotational distributions are predicted on the K PES, in contrast to those calculated on the DK PES. These effects have been explained in terms of the different topology of the entrance and exit channels in the two versions of this surface. Since the available experimental evidence is in conflict with the predicted behavior obtained on the K surface, the likely conclusion is that this surface does not adequately describe the excited $1A''$ state of this system.

The present nonadiabatic calculations based on the QCT-TSH method starting on the DK $2A'$ surface indicate that its contribution to the reactivity is approximately one half of that from the excited $1A''$ state.

ACKNOWLEDGMENTS

We are most grateful to Dr. A. Dobbyn and Professor P. Knowles for providing us with the codes of the DK potential energy surfaces which were computed under Grant No. GR/K41656 of the EPSRC. We also thank Professor Kopin Liu for sending us Refs. 32 and 33 prior to publication. J.F.C. acknowledges financial support through the program ''Acciones para la incorporación de doctores y tecnólogos'' from the Ministry of Education and Culture of Spain. The Computer resources from the Centro de Supercomputación Complutense (Origin 2000) are gratefully acknowledged. This work has been financed by the CICYT of Spain under Contract No. PB98-0763-CO3 and EU Research Training Network ''Reaction Dynamics'' HPRN-CT-1999-00007.

[1] R. Schinke and W. A. Lester, Jr., J. Chem. Phys. **72**, 3754 (1980).
[2] P. A. Whitlock, J. T. Muckerman, and E. R. Fisher, J. Chem. Phys. **76**, 4468 (1982).
[3] G. Durand and X. Chapuisat, Chem. Phys. **96**, 381 (1985).
[4] M. S. Fitzcharles and G. C. Schatz, J. Phys. Chem. **90**, 3634 (1986).
[5] R. Polák, K. Paiderová, and P. J. Kuntz, J. Chem. Phys. **87**, 2863 (1987).
[6] S. P. Walch and L. B. Harding, J. Chem. Phys. **88**, 3629 (1988).
[7] P. J. Kuntz, B. I. Niefer, and J. J. Sloan, J. Chem. Phys. **88**, 3629 (1988).
[8] P. J. Kuntz, B. I. Niefer, and J. J. Sloan, Chem. Phys. **151**, 77 (1991).
[9] T. Peng, D. H. Zhang, J. Z. H. Zhang, and R. Schinke, Chem. Phys. Lett. **248**, 37 (1996).
[10] T.-S. Ho, T. Hollebeek, H. Rabitz, L. B. Harding, and G. C. Schatz, J. Chem. Phys. **105**, 10472 (1996).
[11] G. C. Schatz, A. Papaioannou, L. A. Pederson, L. B. Harding, T. Hollebeek, T. S. Ho, and H. Rabitz, J. Chem. Phys. **107**, 2340 (1997).
[12] J. Dai, J. Chem. Phys. **107**, 4934 (1997).
[13] G. C. Schatz, L. A. Pederson, and P. J. Kuntz, Faraday Discuss. **108**, 357 (1997).
[14] A. J. Alexander, F. J. Aoiz, M. Brouard, and J. P. Simons, Chem. Phys. Lett. **256**, 561 (1996).
[15] A. J. Alexander, F. J. Aoiz, M. Brouard, I. Burak, Y. Fujimura, J. Short, and J. P. Simons, Chem. Phys. Lett. **262**, 589 (1996).
[16] A. J. Alexander, F. J. Aoiz, L. Bañares, M. Brouard, J. Short, and J. P. Simons, J. Phys. Chem. A **101**, 7544 (1997).
[17] A. J. Alexander, D. A. Blunt, M. Brouard, J. P. Simons, F. J. Aoiz, L. Bañares, Y. Fujimura, and M. Tsubouchi, Faraday Discuss. **108**, 375 (1997).
[18] A. J. Alexander, F. J. Aoiz, L. Bañares, M. Brouard, V. J. Herrero, and J. P. Simons, Chem. Phys. Lett. **278**, 313 (1997).
[19] A. J. C. Varandas, A. I. Voronin, A. Riganelli, and P. J. S. B. Caridade, Chem. Phys. Lett. **278**, 325 (1997).
[20] R. J. Buss, P. Casavecchia, T. Hirooka, S. J. Sibener, and Y. T. Lee, Chem. Phys. Lett. **82**, 386 (1981).
[21] D.-C. Che and K. Liu, J. Chem. Phys. **103**, 5164 (1995).
[22] Y.-T. Hsu and K. Liu, J. Chem. Phys. **107**, 1664 (1997).
[23] Y.-T. Hsu, J.-H. Wang, and K. Liu, J. Chem. Phys. **107**, 2351 (1997).
[24] M. Alagia, N. Balucani, L. Cartechini, P. Casavecchia, E. H. van Kleef, G. G. Volpi, P. J. Kuntz, and J. J. Sloan, J. Chem. Phys. **108**, 6698 (1998).
[25] M. Ahmed, D. S. Peterka, and A. G. Suits, Chem. Phys. Lett. **301**, 372 (1999).
[26] A. J. Dobbyn and P. J. Knowles, Mol. Phys. **91**, 1107 (1997); Faraday Discuss. **110**, 247 (1998).
[27] G. G. Balint-Kurti, A. I. González, E. M. Goldfield, and S. K. Gray, Faraday Discuss. **110**, 169 (1998).
[28] S. K. Gray, E. M. Goldfield, G. C. Schatz, and G. G. Balint-Kurti, Phys. Chem. Chem. Phys. **1**, 1141 (1999).
[29] K. Drukker and G. C. Schatz, J. Chem. Phys. **111**, 2451 (1999).
[30] S. K. Gray, C. Petrolongo, K. Drukker, and G. C. Schatz, J. Phys. Chem. A **103**, 9448 (1999).
[31] F. J. Aoiz, L. Bañares, and V. J. Herrero, Chem. Phys. Lett. **310**, 277 (1999).
[32] Y.-T. Hsu, K. Liu, L. A. Pederson, and G. C. Schatz, J. Chem. Phys. **111**, 7921 (1999).
[33] Y.-T. Hsu, K. Liu, L. A. Pederson, and G. C. Schatz, J. Chem. Phys. **111**, 7931 (1999).
[34] S.-H. Lee and K. Liu, J. Chem. Phys. **111**, 4351 (1999).
[35] R. K. Talukdar and A. R. Ravishankara, Chem. Phys. Lett. **253**, 177 (1996).
[36] F. J. Aoiz, L. Bañares, J. F. Castillo, and V. J. Herrero (in preparation).
[37] F. J. Aoiz, L. Bañares, and V. J. Herrero, J. Chem. Soc., Faraday Trans. **94**, 2483 (1998).
[38] J. R. Stine and J. T. Muckerman, J. Chem. Phys. **65**, 3975 (1976).
[39] J. C. Tully, J. Chem. Phys. **93**, 1061 (1990).
[40] J. C. Tully and R. K. Preston, J. Chem. Phys. **55**, 562 (1971); R. K. Preston and J. C. Tully, *ibid.* **54**, 4297 (1971).
[41] W. H. Miller and T. F. George, J. Chem. Phys. **56**, 5637 (1972).
[42] In Ref. 23, a value of $\Gamma(OD/OH)=1.5$ at 0.196 eV collision energy was reported (see the lower panel of Fig. 1 in Ref. 23). However, in Table II of a later work by Lee and Liu on the $S(^1D)+H_2$, D_2, HD reactions [S.-H. Lee and K. Liu, Chem. Phys. Lett. **290**, 323 (1998)], the authors indicated that the cross sections for the $O(^1D)+HD\rightarrow OD+H$ reaction given in Ref. 23 should be scaled up by 1.15. Accordingly, the last value of $\Gamma(OD/OH)$ at $E_{col}=0.196$ eV is 1.73.
[43] J.-B. Song and E. A. Gislason, J. Chem. Phys. **103**, 8444 (1995); **104**, 5834 (1996).
[44] F. J. Aoiz, L. Bañares, J. F. Castillo, and B. Martinez-Haya (in preparation).